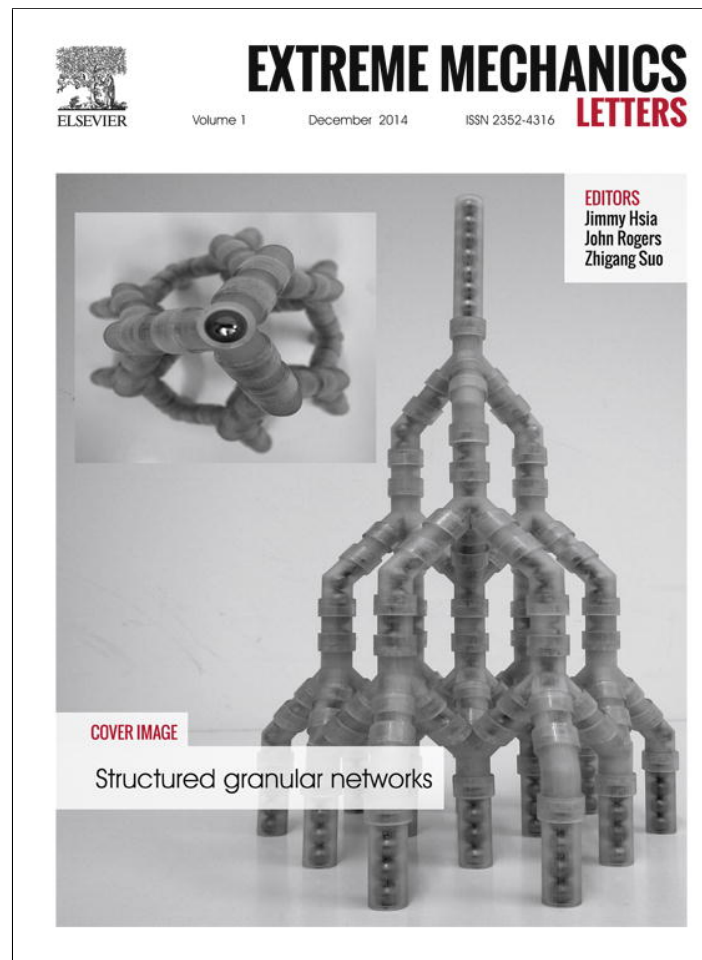


Provided for non-commercial research and education use.
Not for reproduction, distribution or commercial use.



This article appeared in a journal published by Elsevier. The attached copy is furnished to the author for internal non-commercial research and education use, including for instruction at the authors institution and sharing with colleagues.

Other uses, including reproduction and distribution, or selling or licensing copies, or posting to personal, institutional or third party websites are prohibited.

In most cases authors are permitted to post their version of the article (e.g. in Word or Tex form) to their personal website or institutional repository. Authors requiring further information regarding Elsevier's archiving and manuscript policies are encouraged to visit:

<http://www.elsevier.com/authorsrights>

Contents lists available at [ScienceDirect](http://www.sciencedirect.com)

Extreme Mechanics Letters

journal homepage: www.elsevier.com/locate/eml

Directional transport of molecular mass on graphene by straining

Yinjun Huang¹, Shuze Zhu¹, Teng Li^{*}

Department of Mechanical Engineering, University of Maryland, College Park, MD 20742, USA

HIGHLIGHTS

- We reveal a fundamental law of directional transport of molecular mass by straining.
- Directional transport of molecular mass is programmable by devising straining scheme.
- Generally applicable to a wide range of molecular mass and platform materials.

ARTICLE INFO

Article history:

Received 22 October 2014

Received in revised form 5 December 2014

Accepted 5 December 2014

Available online 26 December 2014

Keywords:

Graphene

Molecular mass transport

Strain gradient

Strain engineering

ABSTRACT

Directional transport of molecular mass is essential in enabling desirable functions in nano-devices, but is often challenging to achieve. In this letter, we combine theoretical analysis and molecular simulations to demonstrate a facile mechanism of directional transport of molecular mass on graphene by a simple stretch. We reveal that stretch-induced strain gradient in graphene leads to a net transport force that is sufficient to drive molecular cargo on the graphene in a directional fashion. The large elastic deformability of graphene and the van Der Waals nature of the transport force allow for programmable directional transport of various types of molecular cargo (e.g., graphene flake, carbon nanotube, fullerene, and gold nanoparticle) under the same mechanism. The present findings suggest a fundamental law of directional transport of molecular mass by straining.

© 2014 Elsevier Ltd. All rights reserved.

1. Introduction

Directional transport of molecular mass is of great importance in designing novel molecular devices and machines, and has a wide range of potential applications in fields such as micro/nanofluids and nanorobotics and nanoelectromechanical systems [1–6]. External mechanical, electrical or magnetic excitations have been shown to induce directional motion of molecular mass [2,7–10]. For example, an excited vibrating carbon nanotube cantilever can act as an efficient and simple nanopump [7]. The presence of a gradient in a potential field can also cause directional motion of molecular mass, mimicking the fact that in macroscopic regime objects tend to fall toward lower

gravity potential direction. For example, thermal gradient has been experimentally and theoretically studied on its role of enabling fullerene, graphene flakes, and other molecular cargos to migrate toward lower temperature region on a graphene surface [3,11–13]. Surface chemical gradient, surface tension gradient, surface structural-scale gradient have been demonstrated to be effective to transport water droplet [14–17]. It has been theoretically shown that controlled variations of the intensity or phase of a DC/AC electric field can pump water molecules through carbon nanotubes [18,19]. The above transport mechanisms of molecular mass, however, suffer from either complicated multi-physics actuation scheme, or lack of active control of the transport direction. A facile mechanism of directional transport of molecular mass is still highly desirable.

Introducing strain in graphene by wrinkling [20–22], folding [23–25] and functionalization [26–31] in a programmable fashion have received enormous attention

* Corresponding author.

E-mail address: LiT@umd.edu (T. Li).

¹ These authors contribute equally to this work.

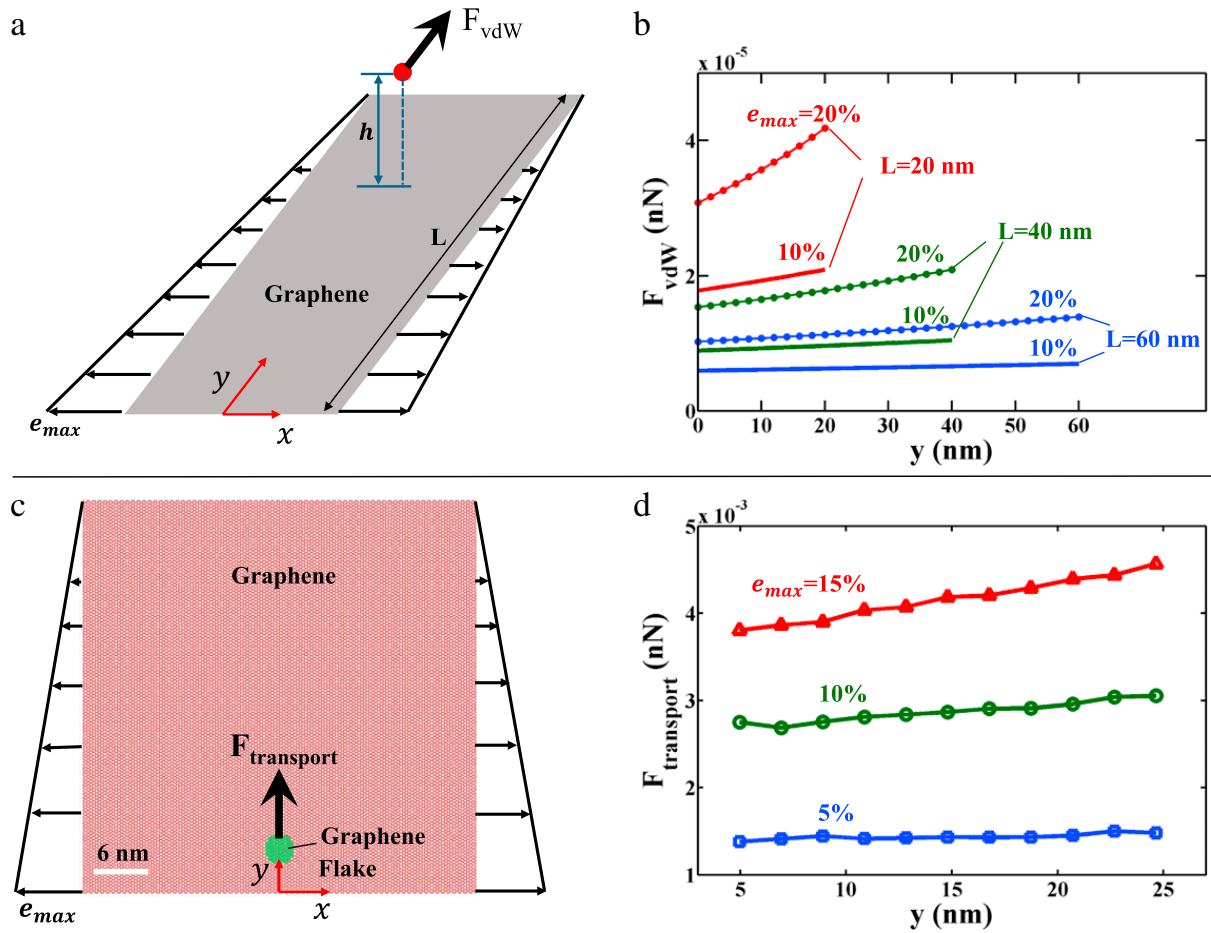


Fig. 1. (a) Schematic showing a net force F_{vdW} acting on an atom (red dot) positioned above on a basal graphene subject to a strain gradient. (b) F_{vdW} as a function of position along y direction for various lengths of basal graphene and strain gradients. (c) Molecular mechanics model of a round graphene flake on a basal graphene subject to a strain gradient to compute the overall net force $F_{transport}$ acting on the graphene flake, which is plotted as a function of position along y direction for various strain gradients (d).

largely due to the need to actively control the electronic and structural properties of graphene [32–38]. Nevertheless few efforts have been made to explore the effect of straining graphene on directional transport of molecular mass. In this Letter, through theoretical modeling and molecular dynamics simulations, we show that a strain gradient in graphene can generate a net transport force on a molecular cargo on the graphene that is sufficient to drive the motion of the molecular cargo in a controlled direction. Given the high elastic deformability of graphene and the facile reversibility of applied straining, programmable transport of molecular mass on graphene can be achieved. The net transport force is essentially van der Waals (vdW) type, therefore such a transport mechanism can be applicable to transport a wide range of molecular cargos. Results from the present study can potentially offer a fundamental law of directional transport of molecular mass by straining.

2. Net transport force on molecular mass induced by a strain gradient in graphene

For an atom positioned above a pristine graphene, the total interaction force between the atom and the graphene can be determined by summing up all atomic-pair potentials between the atom and all carbon atoms in the

graphene. Such a potential for an atomic pair of distance r due to vdW force is usually represented by a Lennard-Jones 6–12 potential, $V(r) = 4\epsilon \left(\frac{\sigma^{12}}{r^{12}} - \frac{\sigma^6}{r^6} \right)$, where $\sqrt[6]{2}\sigma$ is the equilibrium distance between atoms and ϵ is the bond energy at the equilibrium distance. Due to the symmetry of graphene lattice, such a total interaction force zeros out when the atom is positioned with a separation distance from graphene of $h = \sqrt[6]{2}\sigma$. As a result, the atom reaches equilibrium and does not move in a preferred direction. By contrast, when the basal graphene is subject to a strain gradient, the graphene lattice symmetry is broken; there exists a net force acting on the atom, essentially due to the uneven distribution of the carbon atoms in the graphene, as to be detailed below.

Consider a rectangular basal graphene of length L , subject to uniaxial in-plane tension perpendicular to its length direction (Fig. 1(a)). The applied tension linearly decreases from e_{max} at one end to zero at the other end of the graphene. In other words, the graphene is subject to a strain gradient of e_{max}/L . An atom is positioned above the graphene with a separation distance of h . In order to establish a semi-continuum cohesive law between the atom and the graphene, we homogenize carbon atoms in the graphene and represent them by an area density ρ_s . The cohesive energy Φ between the atom and the graphene is

therefore given by [21,39].

$$\Phi = \int V(r) \rho_s dx dy = 4\epsilon \rho_s \pi \left(\frac{\sigma^{12}}{5h^{10}} - \frac{\sigma^6}{2h^4} \right). \quad (1)$$

The relation between the area density ρ_s of deformed graphene under strain (e_x, e_y) and the area density ρ_0 of pristine graphene is given by

$$\rho_s = \frac{\rho_0}{1 + e_x + e_y + e_x e_y} \cong \frac{\rho_0}{1 + e_x + e_y}. \quad (2)$$

Given the uniaxial tension, $e_y = -\nu e_x$, where ν is the Poisson's ratio. This leads to

$$\Phi = \frac{4\epsilon \rho_0 \pi}{1 + (1 - \nu) e_x} \left(\frac{\sigma^{12}}{5h^{10}} - \frac{\sigma^6}{2h^4} \right). \quad (3)$$

A net force acting on the atom from the deformed graphene is then given by

$$F_{vdW} = -\frac{d\Phi}{dy} = \frac{4\epsilon \rho_0 \pi}{(1 + (1 - \nu) e_x)^2} \left(\frac{\sigma^{12}}{5h^{10}} - \frac{\sigma^6}{2h^4} \right) (1 - \nu) \frac{de_x}{dy}. \quad (4)$$

Assuming a linear distribution of uniaxial tension in the graphene, so that

$$e_x = \left(1 - \frac{y}{L}\right) e_{\max}. \quad (5)$$

At the equilibrium separation distance, $h = \sqrt[9]{2}\sigma$. Therefore,

$$F_{vdW} = \frac{\frac{4}{5}\epsilon \rho_0 \pi h^2}{\left(1 + (1 - \nu) \left(1 - \frac{y}{L}\right) e_{\max}\right)^2} (1 - \nu) \frac{e_{\max}}{L} \quad (6)$$

Fig. 1(b) plots F_{vdW} as a function of the location of the atom along y direction, for various lengths of basal graphene (20 nm, 40 nm, and 60 nm, respectively) and e_{\max} (10% and 20%, respectively). Here $\epsilon = 0.00284$ eV, $h = 0.34$ nm, $\rho_0 = \frac{4}{3\sqrt{3}l_0^2}$, $l_0 = 0.142$ nm, which are representative for carbon-carbon vdW interaction. Fig. 1(b) shows that there exists a net force F_{vdW} acting on a carbon atom above a basal graphene subject to a strain gradient, pointing to the decreasing strain direction. In general, a higher strain gradient in the basal graphene (e.g., larger e_{\max} for a fixed L , or shorter L for a fixed e_{\max}) leads to a larger net force. Similarly, for a given e_{\max} , a shorter basal graphene (thus a higher strain gradient) causes a larger net force. F_{vdW} also increases slightly as the location of the atom moves toward the decreasing strain direction. Given that the nature of vdW type interaction, it is expected that such a net force also exists for an atom of different type above a basal graphene subject to a strain gradient.

When a molecular cargo is positioned on a basal graphene under a strain gradient, an overall transport force $F_{transport}$, acting on the cargo and pointing toward the decreasing strain direction, exists and can be computed by summing up all net force acting F_{vdW} on individual atoms in the molecular cargo. To verify the above theoretical consideration, we next perform molecular mechanics simulations to compute $F_{transport}$ acting on a round

graphene flake with a diameter of 2.3 nm above a basal graphene of 30 nm by 30 nm subject to a strain gradient, as shown in Fig. 1(c). With the center of mass of the round graphene flake being hold in the equilibrium position to the basal graphene, energy minimization is performed using large-scale atomic/molecular massively parallel simulator (LAMMPS) [40], in which the carbon material structure is described by the adaptive intermolecular reactive empirical bond order (AIREBO) potential [41]. $F_{transport}$ acting on the graphene flake is computed by summing all carbon-carbon atomic pair potentials between the graphene flake and basal graphene. Fig. 1(d) plots $F_{transport}$ as a function of flake position along y direction for various strain gradients in the basal graphene. A higher strain gradient in the basal graphene leads to a larger overall transport force $F_{transport}$ acting on the graphene flake. $F_{transport}$ also slightly increases as the graphene flake is positioned further along the decreasing strain direction. The molecular mechanics simulation results in Fig. 1(d) are in line with the prediction from the theoretical mechanics model in Fig. 1(a), validating the underlying mechanism of directional transport of molecular mass on graphene via straining. As to be further shown by the molecular dynamics (MD) simulations in the next section, the overall transport force $F_{transport}$ acting on a molecular cargo is sufficient to drive the cargo to move in a controllable fashion on the basal graphene at room temperature.

3. Directional transport of molecular mass on graphene by straining

In this section, we use MD simulations to demonstrate directional transport of various types of molecular mass on a basal graphene by programming the applied strain gradient. All MD simulations are performed using LAMMPS, with the temperature kept at 300 K using canonical ensemble. All carbon material structure is described by the AIREBO potential.

Fig. 2 demonstrates directional transport of a round graphene flake of 2.25 nm in diameter on a graphene nanoribbon (GNR) of 30 nm by 4 nm. Under a strain gradient with $e_{\max} = 15\%$, the net transport force acting on the round graphene flake drives it to start moving toward the decreasing strain direction on the GNR, and reaches the center of the ribbon at 168 ps and the end of the ribbon at 236 ps. The accelerating fashion of the transport process agrees with the steady driving force predicted in Fig. 1(d). Due to the trapping effect of the graphene [42], the round graphene flake bounces back once hitting the zero-strain end of the GNR. The net driving force due to strain gradient further causes the graphene flake to approach the zero-strain end again, arriving with a lower velocity. Eventually the round graphene flake stabilizes around the zero-strain end of the GNR. Upon reversing the direction of strain gradient (with the same amplitude) in the GNR, the net transport force acting on the graphene flake can overcome the trapping effect of the now higher-strain end of the GNR, starting to move in the opposite direction. Once the graphene flake is away from the end of the GNR, the steady net transport force drives it to move in an accelerating fashion. The graphene flake eventually stabilizes at the

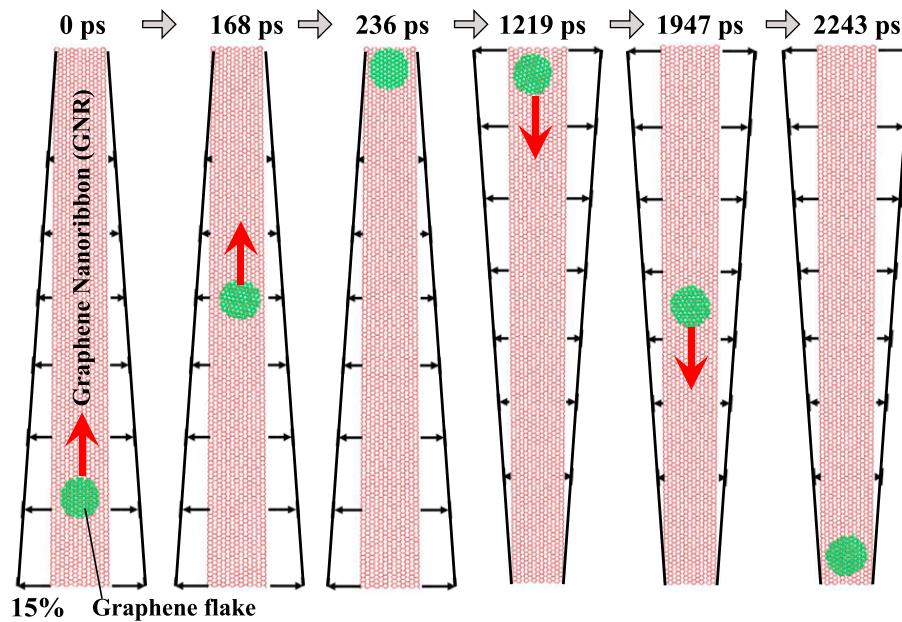


Fig. 2. Snapshots of MD simulations of programmable directional transport of a round graphene flake (green) on a graphene nanoribbon (GNR) by controlling the strain gradient in the GNR. See Supplementary Materials for a simulation video of the transport process (Appendix A).

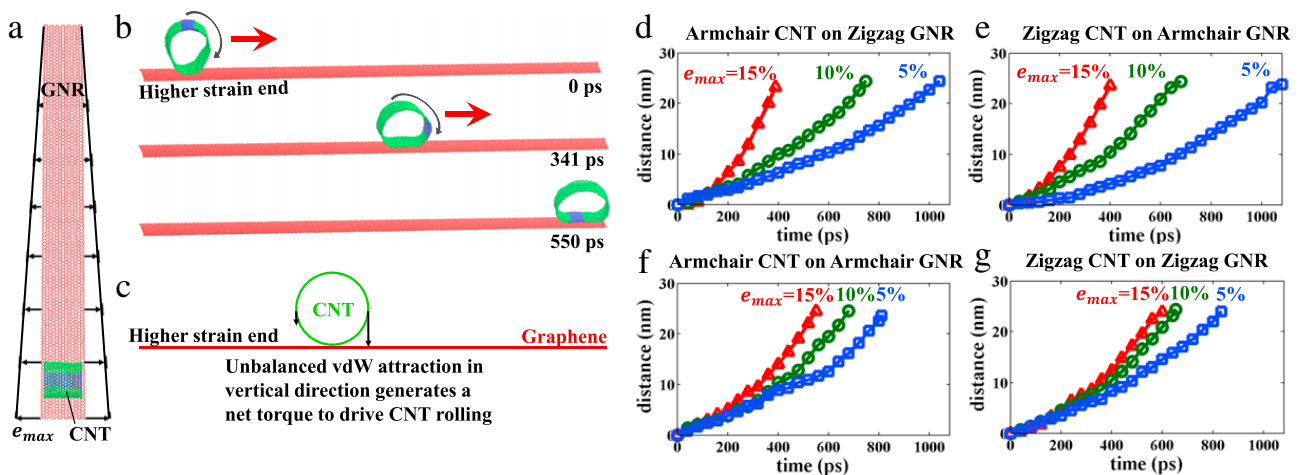


Fig. 3. MD simulations on directional transport of a CNT on a GNR subject to a strain gradient. (a) Schematic of simulation model and applied strain gradient. (b) Snapshots of the transport process of the CNT toward decreasing strain direction. Several rows of carbon atoms in the CNT are shaded in blue to reveal the CNT rolling on the GNR (see Supplementary Materials for a simulation video, Appendix A), resulting from a net torque due to unbalanced vdW attraction in vertical direction acting on the CNT (c). (d)–(g) Transport distance of the CNT as a function of simulation time for various e_{max} and combinations of chirality of the CNT (by its edges) and the GNR (by its longer edges).

zero-strain end of the GNR under the interplay of net transport force and edge trapping effect of graphene. The above simulation case demonstrates that programmable directional transport of molecular mass can be achieved by devising the strain gradient profile in the basal graphene.

Fig. 3 demonstrates directional transport of a carbon nanotube (CNT) on a GNR subject to a strain gradient. A (36, 0) CNT with 2.8 nm in length is positioned at one end of a GNR of 3 nm by 30 nm (Fig. 3(a)). The net transport force on the CNT due to a strain gradient in the GNR with $e_{max} = 15\%$ causes the CNT to migrate on the GNR toward the decreasing strain direction (Fig. 3(b)). By highlighting several rows of carbon atoms in the CNT, it is found that the transport process is achieved by a mixing of sliding and rolling of the CNT on the GNR (see Supplementary Materials for a simulation video, Appendix A). While the

sliding of the CNT on the GNR results from the net transport force pointing to the decreasing strain direction, the rolling of the CNT can be understood as following: The vdW interaction between the CNT and the GNR causes the deformation of the CNT cross-section into a shape with a flat portion in direct contact with the GNR (with an interlayer distance close to that of a graphene bilayer) and the rest curving portion due to the bending rigidity of the CNT cross-section. Away from the equilibrium interlayer distance, the curving portion of the CNT is subject to a vdW attraction from the GNR in the vertical direction. Due to strain-gradient-induced difference in area density of carbon atoms in the GNR (e.g., Eq. (2)), the overall vdW attraction in the vertical direction acting on the half of the CNT at the lower strain side is greater than that at the higher strain side, as illustrated in Fig. 3(c), leading to a net

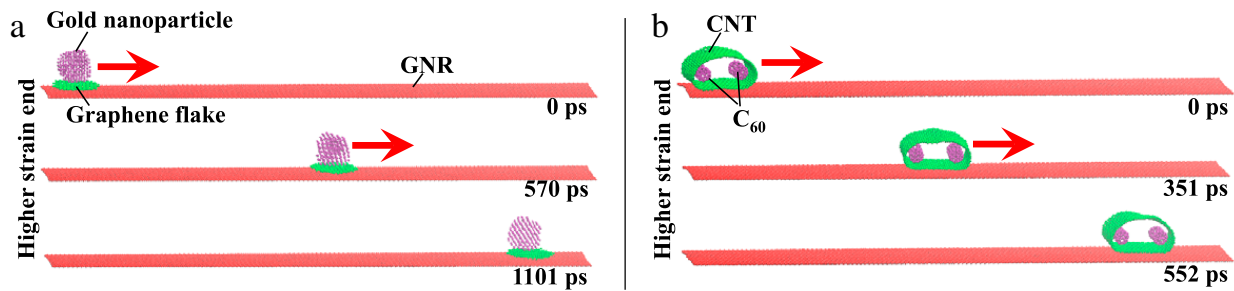


Fig. 4. Molecular dynamics simulations on the directional motion of multiple cargos on a graphene nanoribbon subject to strain gradient (a) a gold nanoparticle on a round graphene flake. (b) Four C_{60} molecules housed in a carbon nanotube.

torque that drives the CNT to roll on the GNR toward the decreasing strain direction.

Further simulations (Fig. 3(d)–(g)) show that the strain-gradient-driven transport of a CNT on a GNR can be effectively achieved for various combinations of CNT and GNR chirality. Given the limiting cases in terms of chirality combinations in Fig. 3(d)–(g), the strain-gradient-driven transport mechanism of CNT on GNR is expected to be robust. Also as shown in Fig. 3(d)–(g), the higher the strain gradient in the GNR (i.e., higher e_{\max} for a fixed GNR length), the faster the transport process, which can be readily accounted to the higher transport force as predicted in Section 2 (e.g., Fig. 1(d)).

Fig. 4 further demonstrates that a graphene flake or a CNT can be used as a vehicle to shuttle other molecular cargo on a GNR under the same mechanism. As shown in Fig. 4(a), a gold nanoparticle with a radius of 1 nm is placed on a round graphene flake with a radius of 1.3 nm sitting on a GNR subject to a strain gradient with $e_{\max} = 10\%$. In the simulations, the gold atoms are described by the embedded atom method (EAM) potential [43], and the vdW interaction between a gold atom and a carbon atom is modeled by Lennard-Jones 6–12 potential, in which [44] $\epsilon_{\text{Au-C}} = 0.0127$ eV, $\sigma_{\text{Au-C}} = 0.2994$ nm, indicating a much stronger interaction between the gold nanoparticle and the round graphene flake than that between the flake and the GNR. The transport force due to strain gradient in the GNR drives the graphene flake to move toward the decreasing strain direction. With the graphene flake moving away from its equilibrium location with the gold nanoparticle, the vdW interaction between them becomes attractive. As a result, the gold nanoparticle is pulled by the graphene flake to start to move toward the decreasing strain direction, while the gold nanoparticle is dragged by the gold nanoparticle to first slow down until stop and then start to move toward the opposite direction. Once the graphene flake moves behind the gold nanoparticle, the vdW interaction between them first slows down the graphene flake to stop and then further drives the flake to move toward the decreasing strain direction again. The above interplay between the graphene flake and the GNR and that between the flake and the gold nanoparticle, on one hand, lead to the overall motion of the cargo (gold)-loaded vehicle (graphene flake) toward the decreasing strain direction; and on the other hand, due to the much larger mass (thus the inertia) of the gold nanoparticle than that of the graphene flake (7.85×10^{-20} g vs. 0.40×10^{-20} g), the graphene flake also oscillates locally back and forth with

respect to the gold nanoparticle (see Supplementary Materials for a simulation video, Appendix A). Fig. 4(b) further shows that a CNT can serve as a vehicle to carry four fullerene (C_{60}) molecules and shuttle them along a GNR subject to a strain gradient with $e_{\max} = 10\%$, in a similar fashion as shown in Fig. 3. With cargo (C_{60}) loaded, the CNT has a larger flat portion than that in Fig. 3, leading to a transport process with more sliding than rolling of the CNT. Nonetheless, simulations in Fig. 4 clearly demonstrates that the strain-gradient-driven transport mechanism can be applicable to achieve directional motion of various type of molecular mass in a programmable fashion.

4. Concluding remarks on strain gradient induced actuation and potential application

The underlying mechanism of strain gradient induced net vdW force is due to the unbalanced atom density in graphene caused by non-uniform strain field. When local strain is lower, the atom density is higher; when local strain is higher, the atom density is lower. Since the vdW force is directly proportional to the atom density, therefore when a graphene surface has a strain gradient, a non-zero net vdW force is expected. Our proposed mechanism can be feasibly extended to design other potential directional motion actuation scheme. For example, two graphene planes forming a channel has been proposed as nanofluid channels [45–48]. As a simple demonstration for such application, we show that strain engineered graphene nanochannel can offer intrinsic actuation force that can potentially pump the molecules moving from one end of the channel to another. Fig. 5(a) shows the morphology of graphene nanochannel with a C_{60} molecule located at the top end. MD simulation is done in 300 K by NVT ensemble. Fig. 5(b) shows the trajectory of the C_{60} molecule. The C_{60} molecule tends to move downwards but also with a horizontal velocity. At 73 ps, C_{60} molecule hits the boundary of the nanochannel. Experiencing a large vdW net force at the edge [42], C_{60} molecule bounces back but still moves downwards. At 100 ps, C_{60} molecule reaches the bottom end and bounces back a shorter distance and then moves downwards again. After several cycles of bouncing upwards and accelerating downwards, eventually the C_{60} molecule is secured at the bottom end of the channel. Such bouncing feature until stabilizing at the bottom, which is analogous to the behavior of a football after being dropped onto the ground in gravity field, strongly suggests that a considerable net vdW force is acting toward the lower

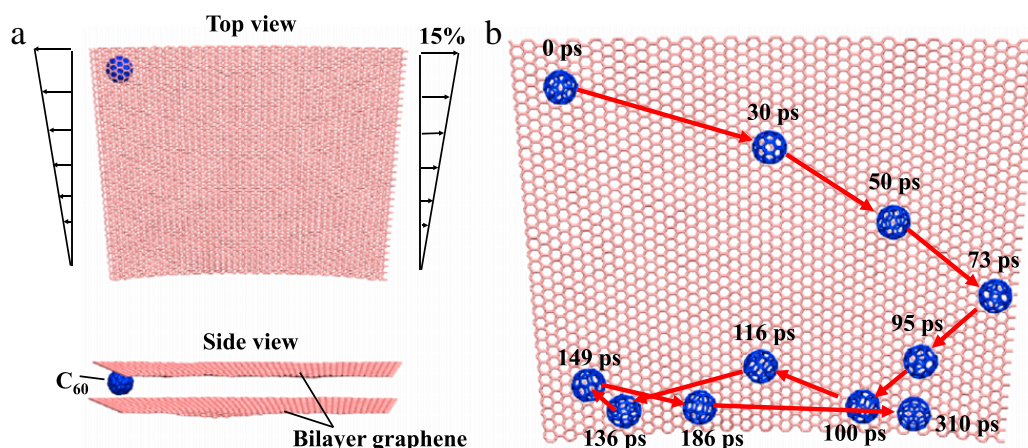


Fig. 5. Molecular dynamics simulations on pumping effect induced by strain engineered graphene nanochannel. (a) Top view and side view of the morphology of a C₆₀ molecule located near the top end of a strain engineered graphene nanochannel at 0 ps. The maximum applied strain is 15%. (b) The trajectory of C₆₀ molecule. For visual clarity, the top graphene layer is not shown.

strain end, indicating a promising solution for the actuation of nanofluids in graphene nanochannels. Therefore we envision that our proposed strain gradient actuation mechanism can open a new pathway for nanoscale actuation.

In reality, graphene may contain defects, such as grain boundaries and cracks, which will in turn affect the deformability of graphene, as demonstrated in recent studies [49]. Furthermore, such defects in graphene could also serve as energy barriers for molecular mass transport [42]. In this sense, graphene with defects is analogous to a pathway with bumps and puddles. Therefore, it is desirable to have high-quality single-crystal graphene as the platform for molecular mass transport. Recently experimental demonstrations of synthesis of large-area single-crystal monolayer are emerging [50], which further suggests the feasibility of the mechanism of directional transport of molecular mass revealed by the present study.

In summary, by combining theoretical analysis and molecular simulations, we demonstrate that a strain gradient in graphene can actuate the directional motion of graphene flakes, carbon nanotubes on its surface. We further demonstrate that flakes and nanotubes can serve as vehicles to transport other cargos. Our proposed strain gradient actuation mechanism can be readily applied to other application scenarios. More comprehensive modeling studies are needed to reveal such new features as well as the effect of temperature, number of basal graphene layers and friction on the transport efficiency. The timescale of the molecular cargo transport is largely affected by the applied strain gradient. As the maximum tensile strain can be applied is limited by the deformability of the basal graphene, the longer the transport path, the smaller the strain gradient, thus the lower the driving force and the slower the transport process. Such a limitation can be mitigated by employing multiple acceleration zones along the path of molecular cargo transport. We therefore call for further systematic simulations and experiments to explore those fertile opportunities.

Acknowledgments

This research is supported by the National Science Foundation (Grant Numbers: 1069076 and 1129826). Y.H

and S.Z. contribute equally to this work. S.Z. thanks the support of the Clark School Future Faculty Program at the University of Maryland (UMD). Y.H. acknowledges the support of UMD Dean's Fellowship.

Appendix A. Supplementary material

Supplementary material related to this article can be found online at <http://dx.doi.org/10.1016/j.eml.2014.12.006>.

References

- [1] Y. Shirai, A. Osgood, Y. Zhao, K. Kelly, J. Tour, Directional control in thermally driven single-molecule nanocars, *Nano Lett.* 5 (2005) 2330–2334.
- [2] T. Kudernac, N. Ruangsapichat, M. Parschau, B. Macia, N. Katsonis, S. Harutyunyan, K. Ernst, B. Feringa, Electrically driven directional motion of a four-wheeled molecule on a metal surface, *Nature* 479 (2011) 208–211.
- [3] A. Barreiro, R. Rurali, E. Hernandez, J. Moser, T. Pichler, L. Forro, A. Bachtold, Subnanometer motion of cargoes driven by thermal gradients along carbon nanotubes, *Science* 320 (2008) 775–778.
- [4] J. Holt, H. Park, Y. Wang, M. Stadermann, A. Artyukhin, C. Grigoropoulos, A. Noy, O. Bakajin, Fast mass transport through sub-2-nanometer carbon nanotubes, *Science* 312 (2006) 1034–1037.
- [5] M. Whitby, N. Quirke, Fluid flow in carbon nanotubes and nanopipes, *Nat. Nanotechnol.* 2 (2007) 87–94.
- [6] G. Whitesides, The origins and the future of microfluidics, *Nature* 442 (2006) 368–373.
- [7] H. Qiu, R. Shen, W. Guo, Vibrating carbon nanotubes as water pumps, *Nano Res.* 4 (2011) 284–289.
- [8] W. Duan, Q. Wang, Water transport with a carbon nanotube pump, *ACS Nano* 4 (2010) 2338–2344.
- [9] X. Li, G. Kong, X. Zhang, G. He, Pumping of water through carbon nanotubes by rotating electric field and rotating magnetic field, *Appl. Phys. Lett.* 103 (2013) 143117.
- [10] Q. Xue, D. Xia, C. Lv, N. Jing, C. Ling, Molecule delivery by the domino effect of carbon nanotubes, *J. Phys. Chem. C* 115 (2011) 20471–20480.
- [11] M. Becton, X. Wang, Thermal gradients on graphene to drive nanoflake motion, *J. Chem. Theory Comput.* 10 (2014) 722–730.
- [12] A. Lohrasebi, M. Neek-Amal, M. Ejtehadi, Directed motion of C-60 on a graphene sheet subjected to a temperature gradient, *Phys. Rev. E* 83 (2011) 042601.
- [13] Z. Guo, T. Chang, X. Guo, H. Gao, Thermal-induced edge barriers and forces in interlayer interaction of concentric carbon nanotubes, *Phys. Rev. Lett.* 107 (2011) 105502.
- [14] S. Hernandez, C. Bennett, C. Junkermeier, S. Tsoi, F. Bezares, R. Stine, J. Robinson, E. Lock, D. Boris, B. Pate, J. Caldwell, T. Reinecke, P. Sheehan, S. Walton, Chemical gradients on graphene to drive droplet motion, *ACS Nano* 7 (2013) 4746–4755.

- [15] L. Zhang, X. Wang, Computational insights of water droplet transport on graphene sheet with chemical density, *J. Appl. Phys.* 115 (2014) 194306.
- [16] M. Chaudhury, G. Whitesides, How to make water run uphill, *Science* 256 (1992) 1539–1541.
- [17] C. Lv, P. Hao, Driving droplet by scale effect on microstructured hydrophobic surfaces, *Langmuir* 28 (2012) 16958–16965.
- [18] K. Rinne, S. Gekle, D. Bonthuis, R. Netz, Nanoscale pumping of water by ac electric fields, *Nano Lett.* 12 (2012) 1780–1783.
- [19] Y. Wang, Y. Zhao, J. Huang, Giant pumping of single-file water molecules in a carbon nanotube, *J. Phys. Chem. B* 115 (2011) 13275–13279.
- [20] M. Yamamoto, O. Pierre-Louis, J. Huang, M. Fuhrer, T. Einstein, W. Cullen, “The princess and the pea” at the nanoscale: wrinkling and delamination of graphene on nanoparticles, *Phys. Rev. X* 2 (2012) 041018.
- [21] S. Zhu, T. Li, Wrinkling instability of graphene on substrate-supported nanoparticles, *J. Appl. Mech.* (2014) 061008.
- [22] Y. Guo, W. Guo, Electronic and field emission properties of wrinkled graphene, *J. Phys. Chem. C* 117 (2013) 692–696.
- [23] S. Cranford, D. Sen, M. Buehler, Meso-origami: folding multilayer graphene sheets, *Appl. Phys. Lett.* 95 (2009) 123121.
- [24] K. Kim, Z. Lee, B. Malone, K. Chan, B. Aleman, W. Regan, W. Gannett, M. Crommie, M. Cohen, A. Zettl, Multiply folded graphene, *Phys. Rev. B* 83 (2011) 245433.
- [25] J. Qi, J. Huang, J. Feng, D. Shi, J. Li, The possibility of chemically inert, graphene-based all-carbon electronic devices with 0.8 eV gap, *ACS Nano* 5 (2011) 3475–3482.
- [26] S. Zhu, T. Li, Hydrogenation enabled scrolling of graphene, *J. Phys. D: Appl. Phys.* 46 (2013) 075301.
- [27] S. Zhu, T. Li, Hydrogenation-assisted graphene origami and its application in programmable molecular mass uptake, storage, and release, *ACS Nano* 8 (2014) 2864–2872.
- [28] D. Yu, F. Liu, Synthesis of carbon nanotubes by rolling up patterned graphene nanoribbons using selective atomic adsorption, *Nano Lett.* 7 (2007) 3046–3050.
- [29] D. Boukhvalov, M. Katsnelson, A. Lichtenstein, Hydrogen on graphene: electronic structure, total energy, structural distortions and magnetism from first-principles calculations, *Phys. Rev. B* 77 (2008) 035427.
- [30] D. Elias, R. Nair, T. Mohiuddin, S. Morozov, P. Blake, M. Halsall, A. Ferrari, D. Boukhvalov, M. Katsnelson, A. Geim, K. Novoselov, Control of graphene's properties by reversible hydrogenation: evidence for graphane, *Science* 323 (2009) 610–613.
- [31] J. Zhou, Q. Wang, Q. Sun, X. Chen, Y. Kawazoe, P. Jena, Ferromagnetism in semihydrogenated graphene sheet, *Nano Lett.* 9 (2009) 3867–3870.
- [32] N. Levy, S. Burke, K. Meaker, M. Panlasigui, A. Zettl, F. Guinea, A. Neto, M. Crommie, Strain-induced pseudo-magnetic fields greater than 300 tesla in graphene nanobubbles, *Science* 329 (2010) 544–547.
- [33] K. Kim, Y. Blanter, K. Ahn, Interplay between real and pseudomagnetic field in graphene with strain, *Phys. Rev. B* 84 (2011) 081401(R).
- [34] F. De Juan, J. Manes, M. Vozmediano, Gauge fields from strain in graphene, *Phys. Rev. B* 87 (2013) 165131.
- [35] J. Sloan, A. Sanjuan, Z. Wang, C. Horvath, S. Barraza-Lopez, Strain gauge fields for rippled graphene membranes under central mechanical load: an approach beyond first-order continuum elasticity, *Phys. Rev. B* 87 (2013) 155436.
- [36] N.N. Klimov, S. Jung, S. Zhu, T. Li, C.A. Wright, S.D. Solares, D.B. Newell, N.B. Zhitenev, J.A. Stroscio, Electromechanical properties of graphene drumheads, *Science* 336 (2012) 1557–1561.
- [37] F. Guinea, M. Katsnelson, A. Geim, Energy gaps and a zero-field quantum hall effect in graphene by strain engineering, *Nat. Phys.* 6 (2010) 30–33.
- [38] S. Zhu, Y. Huang, N.N. Klimov, D.B. Newell, N.B. Zhitenev, J.A. Stroscio, S.D. Solares, T. Li, Pseudomagnetic fields in a locally strained graphene drumhead, *Phys. Rev. B* 90 (2014) 075426.
- [39] L. Jiang, Y. Huang, H. Jiang, G. Ravichandran, H. Gao, K. Hwang, B. Liu, A cohesive law for carbon nanotube/polymer interfaces based on the van der Waals force, *J. Mech. Phys. Solids* 54 (2006) 2436–2452.
- [40] S. Plimpton, Fast parallel algorithms for short-range molecular-dynamics, *J. Comput. Phys.* 117 (1995) 1–19.
- [41] S. Stuart, A. Tutein, J. Harrison, A reactive potential for hydrocarbons with intermolecular interactions, *J. Chem. Phys.* 112 (2000) 6472.
- [42] Y. Huang, S. Zhu, T. Li, Line defects guided molecular patterning on graphene, *Appl. Phys. Lett.* 104 (2014) 093102.
- [43] S. Foiles, M. Baskes, M. Daw, Embedded-atom-method functions for the fcc metals Cu, Ag, Au, Ni, Pd, Pt, and their alloys, *Phys. Rev. B* 33 (1986) 7983.
- [44] S. Arcidiacono, J. Walther, D. Poulidakos, D. Passerone, P. Koumoutsakos, Solidification of gold nanoparticles in carbon nanotubes, *Phys. Rev. Lett.* 94 (2005) 105502.
- [45] W. Xiong, J. Liu, M. Ma, Z. Xu, J. Sheridan, Q. Zheng, Strain engineering water transport in graphene nanochannels, *Phys. Rev. E* 84 (2011) 056329.
- [46] L. Liu, L. Zhang, Z. Sun, G. Xi, Graphene nanoribbon-guided fluid channel: a fast transporter of nanofluids, *Nanoscale* 4 (2012) 6279–6283.
- [47] S. Kannam, B. Todd, J. Hansen, P. Davis, Slip flow in graphene nanochannels, *J. Chem. Phys.* 135 (2011) 144701.
- [48] Y. Qiao, X. Xu, H. Li, Conduction of water molecules through graphene bilayer, *Appl. Phys. Lett.* 103 (2013) 233106.
- [49] P. Zhang, L.L. Ma, F.F. Fan, Z. Zeng, C. Peng, P.E. Loya, Z. Liu, Y.J. Gong, J.N. Zhang, X.X. Zhang, P.M. Ajayan, T. Zhu, J. Lou, Fracture toughness of graphene, *Nature Commun.* 5 (2014) 3782.
- [50] J.H. Lee, E.K. Lee, W.J. Joo, Y. Jang, B.S. Kim, J.Y. Lim, S.H. Choi, S.J. Ahn, J.R. Ahn, M.H. Park, C.W. Yang, B.L. Choi, S.W. Hwang, D. Whang, Wafer-scale growth of single-crystal monolayer graphene on reusable hydrogen-terminated germanium, *Science* 344 (2014) 286–289.